

# Tricritical transition in the classical $XY$ model on Kagomé lattice under local anisotropy

Farhad Shahbazi <sup>\*</sup>, Saba Mortezaipoor <sup>†</sup>

*Dept. of Physics , Isfahan University of Technology, 84156-83111, Isfahan, Iran.*

## Abstract

Using mean-field theory and high resolution Monte Carlo simulation technique based on multi-histogram method, we have investigated the critical properties of an antiferromagnetic  $XY$  model on the 2D Kagomé lattice, with single ion easy-axes anisotropy. The mean-field theory predicts second-order phase transition from disordered to all-in all-out state for any value of anisotropy for this model. However, Monte Carlo simulations result in first order transition for small values of anisotropy which turns to second order with increasing strength of anisotropy, indicating the existence of a tricritical point for this model. The critical exponents, obtained by finite-size scaling methods, show that the transition is in Ising universality class for large values of anisotropy, while the critical behaviour of the system deviates from  $2D-\phi^6$  model near the tricritical point. This suggests the possibility for existence of a new tricritical universality in two-dimensions.

PACS numbers: 75.30.Gw, 75.30.Kz, 68.35.Rh, 64.60.Fr

---

<sup>\*</sup>Electronic address: shahbazi@cc.iut.ac.ir

<sup>†</sup>Electronic address: mortezaipoor-s@ph.iut.ac.ir

## I. INTRODUCTION

The phenomenon of geometric frustration has attracted the interest of physicists due to the presence of degeneracy in the classical ground states arising from the arrangement of spins on triangular clusters [1–4]. A frustrated magnet is one in which not all interaction energies can be simultaneously optimized, for which the anti-ferromagnetic Ising model on a two-dimensional triangular lattice, is an example. The highly frustrated magnets, on the other hand, are the class of frustrated magnets that have an infinite number of classical ground states, even after removing the global symmetries of Hamiltonian.

The classical  $XY$  anti-ferromagnet on the two-dimensional Kagomé lattice constructed from corner-sharing triangular units and the classical Heisenberg antiferromagnet on the  $3D$  pyrochlore lattice consisting of corner-sharing tetrahedra are two prototypes of the highly frustrated class. The discoveries, such as heavy-fermion behaviour [5], spin-ice ordering [6–8], spin nematics [9], spin liquid behaviours [10–12] and even novel superconductivity [13] in materials with magnetic sublattices of corner-sharing tetrahedra (such as spinel and pyrochlores), have made these structures in the focus of physicists’s attention over the recent years.

It has been widely accepted that no order-by-disorder mechanism can establish a long-range order in the Heisenberg pyrochlore anti-ferromagnet, consequently such a system remains disordered at all temperatures [14–16]. However, experimental observations have represented an all-in all-out long-range order (consisting of four sublattices oriented along four [111] spin directions), for the low-temperature phase of  $\text{FeF}_3$  in pyrochlore form [17,18]. In this compound, the  $\text{Fe}^{+3}$  ions located on a pyrochlore lattice, interact anti-ferromagnetically with their nearest neighbors. Since, the magnetic  $\text{Fe}^{+3}$  ions are in  $d^5$  electronic configuration with a totally symmetric ground state and no net angular momentum, this system can be considered as a Heisenberg anti-ferromagnet and so the origin of the long-range ordered phase in it, has remained as a puzzle. Reimers *et al* have shown that, taking into account the interaction with farther neighbors, would cause a second order transition in this a sys-

tem [19]. However, they found that because of the thermal fluctuations, a co-linear spin ordering would be preferred rather than the all-in all-out state. Therefore, it seems that to stabilize a long range all-in all-out spin configuration, one should inevitably introduce a single-ion an-isotropic crystal field term in the model Hamiltonian. Another interesting aspect of the transition in  $\text{pyr-Fe}^{+3}$  is in its universality class. The order parameter critical exponent  $\beta$  has been fixed to the value 0.18(2), in neutron- diffraction experiments, which is nearest to the tetra-critical value  $\beta = 1/6$  [20]. On the other hand, recent Monte Carlo simulations, carried on Heisenberg pyrochlore antiferromagnet with single ion anisotropy, have revealed the existence of a tricritical point for this system [21,22].

The above interesting problem motivated us to study the critical properties of its two-dimensional equivalent, the  $XY$  Kagomé anti-ferromagnet model with single-ion anisotropy. The classical antiferromagnetic  $O(n)$  models on the Kagomé lattice have been studied by Huse and Rutenberg [23]. There, it has been shown that the Ising model ( $n = 1$ ) is disordered at all temperatures, while the  $XY$  model ( $n = 2$ ) represents quasi long-range order in a three-fold ordered parameter at zero temperature. Because the system is two-dimensional this quasi long-range order does not survive at finite temperatures and so transforms to disordered phase through a Kosterlitz-Thouless transition. The ground state of the  $XY$  model has the same properties as the three-state Potts model which can be mapped exactly onto solid-on solid (SOS) model at the roughening transition. On the other hand, the study of two-dimensional antiferromagnet Heisenberg model on Kagomé, have been carried out by Ritchey *et al*, which resulted in a coplanar spin configurations in which there are nematic spin correlations with planar threefold symmetry and non-Abelian homotopy [24]. They have also shown that very small amounts of bond  $XY$  anisotropy are sufficient to convert a crossover to a topological phase transition, in which the binding of non-Abelian disclinations would result in a glassy behavior in the absence of extrinsic disorder.

The Hamiltonian of nearest-neighbor  $XY$  antiferromagnet model on the Kagomé lattice is given by:

$$H = -J \sum_{\langle ij \rangle} \mathbf{S}_i \cdot \mathbf{S}_j, \quad (1)$$

in which  $J < 0$  and  $\mathbf{S}_i$  denotes the unit planar vectors and  $\langle ij \rangle$  indicates the nearest-neighbors. The ground state of this model is known to have a huge accidental degeneracy not related to the global symmetries of the Hamiltonian [23,25]. In any ground state of the Kagomé lattice the spins  $\mathbf{S}_i$  acquires only three directions whose angles with respect to an arbitrary axis, say  $x$ -axis, differ from each other by  $2\pi/3$ . Therefore, the ground state in addition to the continuous  $U(1)$  symmetry (due to the arbitrary simultaneous rotation of all spins) is characterized by a well developed discrete degeneracy of the same type as in the 3-state antiferromagnetic Potts model.

The extensive degeneracy of the ground state in this model makes it extremely unstable towards the imposing of perturbations [26]. For instance, if one adds a single-ion easy-axis anisotropic term to Hamiltonian (1), all spins prefer to align along the anisotropy directions yielding a long-range all-in all-out state for the system.

The goal of this paper is to determine the critical properties of an  $XY$  model on the two dimensional Kagomé lattice with single ion easy-axes anisotropic term. For this purpose we employ mean-field theory and Monte Carlo simulation.

The structure of paper is as follows. In Sec. II, we introduce a mean-field formalism to derive the qualitative picture of transitions in the model. Section III is dedicated to the Monte Carlo method based on multiple histograms and also some methods for analyzing the Monte Carlo data to determine the order of transitions, critical temperatures and critical exponents. The simulation results and discussion are given in Sec. IV and conclusion appears in Sec. V.

## II. MEAN-FIELD FORMALISM

The Hamiltonian, describing the  $XY$  spins with nearest-neighbor anti-ferromagnetic interaction on a Kagomé lattice subjected to single site easy-axes anisotropy, is given by :

$$H = -\frac{J}{2} \sum_{i,j} \sum_{a,b} \mathbf{S}_i^a \cdot \mathbf{S}_j^b - D \sum_i \sum_a (\mathbf{S}_i^a \cdot \hat{\mathbf{z}}^a)^2, \quad (2)$$

in which  $J < 0, D > 0$  and  $i, j = 1, \dots, N$  and  $a, b = 1, 2, 3$  denote the Bravais lattice and sublattice indices, respectively.  $\hat{\mathbf{z}}^a$ 's represent the unit vectors of three easy-axes directions in 2d plane, which are along the line connecting the corner and the center of corner-sharing triangular units, given by:

$$\begin{aligned} \hat{\mathbf{z}}^1 &= \left( \frac{\sqrt{3}}{2}, \frac{-1}{2} \right) \\ \hat{\mathbf{z}}^2 &= \left( -\frac{\sqrt{3}}{2}, \frac{-1}{2} \right) \\ \hat{\mathbf{z}}^3 &= (0, 1) \end{aligned} \quad (3)$$

in global Cartesian coordinates.

To apply mean-field theory on this model, we follow the method introduced by Harris, Mouritson and Berlinsky [19,27]. Defining the average magnetization as  $\mathbf{M}_i^{\mathbf{a}} = \langle \mathbf{S}_i^{\mathbf{a}} \rangle$  and the deviation from the mean magnetization as  $\delta \mathbf{S}_i^a = \mathbf{S}_i^{\mathbf{a}} - \mathbf{M}_i^{\mathbf{a}}$ , to order  $O(\delta S^2)$ , we can write the Hamiltonian (Eq.(2)) as the following linear form:

$$H = \frac{J}{2} \sum_{i,j} \sum_{a,b} \mathbf{M}_i^a \cdot \mathbf{M}_j^b + D \sum_i \sum_a (\mathbf{M}_i^a \cdot \hat{\mathbf{z}}^a)^2 - J \sum_{i,a} \sum_{j,b} \mathbf{M}_j^b \cdot \mathbf{S}_i^a - 2D \sum_{i,a} (\mathbf{S}_i^a \cdot \hat{\mathbf{z}}^a) (\mathbf{M}_i^a \cdot \hat{\mathbf{z}}^a). \quad (4)$$

Therefore, the mean-field partition function can be written as:

$$Z = e^{-\beta \left( \frac{J}{2} \sum_{i,j} \sum_{a,b} \mathbf{M}_i^a \cdot \mathbf{M}_j^b + D \sum_i \sum_a (\mathbf{M}_i^a \cdot \hat{\mathbf{z}}^a)^2 \right)} \prod_{i,a} \int e^{\beta \mathbf{B}_i^a \cdot \mathbf{S}_i^a} d\mathbf{S}_i^a, \quad (5)$$

where

$$\mathbf{B}_i^a = J \sum_{j \neq i} \sum_{b \neq a} \mathbf{M}_j^b + 2D (\mathbf{M}_i^a \cdot \hat{\mathbf{z}}^a) \hat{\mathbf{z}}^a, \quad (6)$$

in which, the summation is over the nearest neighbors. The integral in Eq.(5) can be evaluated easily as follows:

$$\int e^{\beta \mathbf{B}_i^a \cdot \mathbf{S}_i^a} d\mathbf{S}_i^a = 2\pi \int_0^\pi e^{\beta B_i^a \cos(\theta)} d\theta = 2\pi I_0(\beta B_i^a), \quad (7)$$

where  $B_i^a = |\mathbf{B}_i^a|$ . Then, assuming  $K_B = 1$ , we reach the following expression for the free energy:

$$F = -T \ln Z = \frac{J}{2} \sum_{i,j} \sum_{a,b} \mathbf{M}_i^a \cdot \mathbf{M}_j^b + D \sum_i \sum_a (\mathbf{M}_i^a \cdot \hat{\mathbf{z}}^a)^2 - T \sum_{i,a} \ln \left( 2\pi I_0 \left( \frac{B_i^a}{T} \right) \right). \quad (8)$$

From the mean-field free energy, obtained above, one can calculate the magnetization and entropy as:

$$S = -\frac{\partial F}{\partial T} = \sum_{i,a} \ln \left( 2\pi I_0 \left( \frac{B_i^a}{T} \right) \right) + \frac{1}{T^2} \sum_{i,a} \frac{B_i^a I_1 \left( \frac{B_i^a}{T} \right)}{2I_0 \left( \frac{B_i^a}{T} \right)} \quad (9)$$

$$, \mathbf{M}_i^a = -\nabla_B F = -\frac{\partial F}{\partial B_i^a} \hat{B}_i^a = -\sum_{i,a} \frac{I_1 \left( \frac{B_i^a}{T} \right)}{2I_0 \left( \frac{B_i^a}{T} \right)}. \quad (10)$$

For small values of  $B$ , one can expand Eq.(10) as:

$$M_i^a = \left[ \frac{B_i^a}{2T} - \frac{B_i^{a3}}{16T^3} + \frac{B_i^{a5}}{96T^5} - \frac{11}{6144} \frac{B_i^{a7}}{T^7} + O(B^9) \right], \quad (11)$$

from which, by reversing the series one gets:

$$B_i^a = 2TM_i^a - T(M_i^a)^3 + \frac{5}{9}(M_i^a)^5 + O(M^8). \quad (12)$$

Substituting Eq.(12) into Eq.(9) and expanding the entropy in powers of  $M_i^a$ , enables us to expand the free energy as:

$$\begin{aligned} F &= \langle H \rangle - TS \\ &= -4NT \ln(4\pi) - \frac{J}{2} \sum_{i,j} \sum_{a,b} \mathbf{M}_i^a \cdot \mathbf{M}_j^b - D \sum_{i,a} (\mathbf{M}_i^a \cdot \hat{\mathbf{z}}^a)^2 \\ &\quad + T \sum_{i,a} \left( (M_i^a)^2 + \frac{1}{4}(M_i^a)^4 - \frac{5}{36}(M_i^a)^6 + O(M^7) \right), \end{aligned} \quad (13)$$

where we have used Eq.(4). We can also expand the free energy in terms of Fourier components defined by:

$$\mathbf{M}_i^a = \sum_{\mathbf{q}} \mathbf{M}_{\mathbf{q}}^a \exp(i\mathbf{q} \cdot \mathbf{R}_i^a) \quad (14)$$

$$J_{\mathbf{q}}^{ab} = \sum_{j \neq i} \sum_{b \neq a} J \exp \left( i\mathbf{q} \cdot (\mathbf{R}_i^a - \mathbf{R}_j^b) \right), \quad (15)$$

where the summation in Eq.(15) is over the nearest neighbors of a selected spins. Then we reach the following form for the free energy per particle in terms of Fourier components:

$$\begin{aligned}
f(T, J, D) &= \frac{F(T, J, D)}{N} = -4T \ln(4\pi) \\
&+ \frac{1}{2} \sum_q \sum_{ab} \mathbf{M}_{\mathbf{q}}^a \mathbf{M}_{-\mathbf{q}}^b (2T \delta^{ab} - J_{\mathbf{q}}^{ab}) - D \sum_q \sum_a (\mathbf{M}_{\mathbf{q}}^a \cdot \hat{z}^a) (\mathbf{M}_{-\mathbf{q}}^a \cdot \hat{z}^a) \\
&+ \frac{1}{4} T \sum_a \sum'_{\{\mathbf{q}\}} (\mathbf{M}_{\mathbf{q}1}^a \cdot \mathbf{M}_{\mathbf{q}2}^a) (\mathbf{M}_{\mathbf{q}3}^a \cdot \mathbf{M}_{\mathbf{q}4}^a) \\
&- \frac{5}{36} T \sum_a \sum'_{\{\mathbf{q}\}} (\mathbf{M}_{\mathbf{q}1}^a \cdot \mathbf{M}_{\mathbf{q}2}^a) (\mathbf{M}_{\mathbf{q}3}^a \cdot \mathbf{M}_{\mathbf{q}4}^a) (\mathbf{M}_{\mathbf{q}5}^a \cdot \mathbf{M}_{\mathbf{q}6}^a) + O(M^7), \tag{16}
\end{aligned}$$

where

$$\sum'_{\{\mathbf{q}\}} = \sum_{\{\mathbf{q}\}} \delta(\sum_i \mathbf{q} \mathbf{i}).$$

The free energy (Eq.16) can be rewritten in terms of Cartesian components of  $\mathbf{M}_{\mathbf{q}}^a = (m_{\mathbf{q}}^{a,1}, m_{\mathbf{q}}^{a,2})$  as:

$$\begin{aligned}
f(T, J, D) &= -4T \ln(4\pi) + \frac{1}{2} \sum_q \sum_{ab} \sum_{\alpha\beta} (2T \delta^{ab} \delta^{\alpha\beta} - J_{\mathbf{q}}^{ab} \delta^{\alpha\beta} - D_{\alpha\beta}^a \delta^{ab}) m_{\mathbf{q}}^{a,\alpha} m_{-\mathbf{q}}^{b,\beta} \\
&+ \frac{1}{4} T \sum_a \sum_{\alpha\beta} \sum'_{\{\mathbf{q}\}} (m_{\mathbf{q}1}^{a,\alpha} m_{\mathbf{q}2}^{a,\alpha}) (m_{\mathbf{q}3}^{a,\beta} m_{\mathbf{q}4}^{a,\beta}) \\
&- \frac{5}{36} T \sum_a \sum_{\alpha\beta\gamma} \sum'_{\{\mathbf{q}\}} (m_{\mathbf{q}1}^{a,\alpha} m_{\mathbf{q}2}^{a,\alpha}) (m_{\mathbf{q}3}^{a,\beta} m_{\mathbf{q}4}^{a,\beta}) (m_{\mathbf{q}5}^{a,\gamma} m_{\mathbf{q}6}^{a,\gamma}) + O(M^7), \tag{17}
\end{aligned}$$

in which  $\alpha, \beta, \gamma$  take the values 1, 2. It can be seen from the above equation, that only the an-isotropic term  $D$  couples the different Cartesian components of  $\mathbf{M}$ . The  $2 \times 2$  matrices  $D^a$  are given by:

$$D^1 = D \begin{pmatrix} \frac{\sqrt{3}}{2} & \frac{\sqrt{3}}{4} \\ \frac{\sqrt{3}}{4} & \frac{1}{2} \end{pmatrix}, D^2 = D \begin{pmatrix} \frac{\sqrt{3}}{2} & -\frac{\sqrt{3}}{4} \\ -\frac{\sqrt{3}}{4} & \frac{1}{2} \end{pmatrix}, D^3 = D \begin{pmatrix} 0 & 0 \\ 0 & 1 \end{pmatrix}. \tag{18}$$

Thus we are left with the following coupling  $6 \times 6$  matrix for the quadratic terms:

$$\tilde{J}_{\mathbf{q}} = D \begin{pmatrix} D^1 & J_{\mathbf{q}}^{12} & J_{\mathbf{q}}^{13} \\ J_{\mathbf{q}}^{12} & D^2 & J_{\mathbf{q}}^{23} \\ J_{\mathbf{q}}^{13} & J_{\mathbf{q}}^{23} & D^3 \end{pmatrix}, \tag{19}$$

in which the off-diagonal matrices  $J_{\mathbf{q}}^{ij}$  are proportional to the  $2 \times 2$  unit matrix as follows :

$$J_{\mathbf{q}}^{12} = 2J \cos\left(\frac{q_x}{2}\right) I_{2 \times 2} \quad (20)$$

$$J_{\mathbf{q}}^{13} = 2J \cos\left(\frac{\sqrt{3}q_y + q_x}{2}\right) I_{2 \times 2} \quad (21)$$

$$J_{\mathbf{q}}^{23} = 2J \cos\left(\frac{\sqrt{3}q_y - q_x}{2}\right) I_{2 \times 2}. \quad (22)$$

In deriving the above expressions, we have used Eq.(15) together with the positions of Kagomé atoms given by their  $xy$  components. For convenience we reduce the number of indices ( $a = 1, 2, 3$  and  $\alpha = 1, 2$ ) by defining a new set of indices  $s = 1, \dots, 6$ , which leads to a 6-component magnetization vector as:

$$\tilde{\mathbf{M}}_{\mathbf{q}} = (m_{\mathbf{q}}^{1,1}, m_{\mathbf{q}}^{1,2}, m_{\mathbf{q}}^{2,1}, \dots, m_{\mathbf{q}}^{3,2}) = (m_{\mathbf{q}}^1, m_{\mathbf{q}}^2, \dots, m_{\mathbf{q}}^6), \quad (23)$$

from which the quadratic term in free energy can be written as:

$$f^{(2)} = \sum_{\mathbf{q}} \tilde{\mathbf{M}}_{\mathbf{q}} \cdot \tilde{J}_{\mathbf{q}} \cdot \tilde{\mathbf{M}}_{\mathbf{q}}^T. \quad (24)$$

Diagonalizing the quadratic term, requires transforming to the normal modes  $\Phi_{\mathbf{q}}$ :

$$m_{\mathbf{q}}^s = \sum_{i=1}^6 U_{\mathbf{q}}^{si} \phi_{\mathbf{q}}^i \quad (25)$$

for  $s = 1, 2, \dots, 6$ .

$U_{\mathbf{q}}$  is the unitary matrix that diagonalizes the coupling matrix  $\tilde{J}_{\mathbf{q}}$ , with eigenvalues  $\lambda_{\mathbf{q}}^i$ :

$$\sum_b \tilde{J}_{\mathbf{q}}^{ab} U_{\mathbf{q}}^{bi} = \lambda_{\mathbf{q}}^i U_{\mathbf{q}}^{ai}. \quad (26)$$

in which, the unitarity condition requires:

$$\sum_a U_{\mathbf{q}}^{ai} U_{-\mathbf{q}}^{aj} = \delta^{ij}. \quad (27)$$

Equation (26) enables us to write the free energy as a power series in terms of normal modes, such that to  $O(\phi^7)$  we obtain the following expansion for the free energy:



$$\begin{aligned}
f(T, J, D) = & -4T \ln(4\pi) + \frac{1}{2} \sum_q \sum_{i=1}^{12} (2T - \lambda_{\mathbf{q}}^i) \phi_{\mathbf{q}}^i \phi_{-\mathbf{q}}^i \\
& + \frac{T}{4} \sum_{s=1}^{12} \sum_{ijkl} \sum_{\{\mathbf{q}\}}' U_{\mathbf{q}1}^{si} U_{\mathbf{q}2}^{sj} U_{\mathbf{q}3}^{sk} U_{\mathbf{q}4}^{sl} \phi_{\mathbf{q}1}^i \phi_{\mathbf{q}2}^j \phi_{\mathbf{q}3}^k \phi_{\mathbf{q}4}^l \\
& + \frac{5}{36} T \sum_{s=1}^{12} \sum_{ijklmn} \sum_{\{\mathbf{q}\}}' U_{\mathbf{q}1}^{si} U_{\mathbf{q}2}^{sj} U_{\mathbf{q}3}^{sk} U_{\mathbf{q}4}^{sl} U_{\mathbf{q}5}^{sm} U_{\mathbf{q}6}^{sn} \phi_{\mathbf{q}1}^i \phi_{\mathbf{q}2}^j \phi_{\mathbf{q}3}^k \phi_{\mathbf{q}4}^l \phi_{\mathbf{q}5}^m \phi_{\mathbf{q}6}^n.
\end{aligned} \tag{28}$$

It is clear that phase transition occurs when the sign of quadratic term of free energy changes. Therefore, from the above expression one finds that the spontaneously breaking symmetry occurs at a temperature:

$$T_c = \frac{1}{2} \max_{\mathbf{q}, i} \{\lambda_{\mathbf{q}}^i\}, \tag{29}$$

where  $\max \{\}$  means the global maximum over all  $i$  and  $\mathbf{q}$ . In the case of  $D = 0$  one can exactly diagonalize the matrix  $\tilde{J}_{\mathbf{q}}$  (Eq.(19)) and find the following eigenvalues:

$$\begin{aligned}
\lambda_{\mathbf{q}}^i &= -2J & i &= 1, 2 \\
\lambda_{\mathbf{q}}^i &= 2J(1 - \sqrt{3 + Q}) & i &= 3, 4 \\
\lambda_{\mathbf{q}}^i &= 2J(1 + \sqrt{3 + Q}) & i &= 5, 6,
\end{aligned} \tag{30}$$

where  $Q$  is given by:

$$Q = \{\cos(2q_x) + \cos(\sqrt{3}q_x + q_y) + \cos((2 - \sqrt{3})q_x - q_y)\}, \tag{31}$$

which coincides with the result derived in Ref. [19]. The above results show that for  $J < 0$  the largest eigenvalues are degenerate and dispersionless ( $q$ -independent), such that when  $T < -J$ , the order parameters corresponding to all of these modes turn to be nonzero and we were left with a huge number of states with broken symmetry. Therefore, because of the extensive degeneracy of symmetry broken states, one concludes that in mean-field theory, no long range order can be established as the temperature decreases down to zero. The  $q$ -dependence of eigenvalues for  $D = 0$  along  $[1\ 0]$  direction is depicted in Fig.(1).

For an-isotropic case ( $D > 0$ ) the eigenvalues of matrix  $\tilde{J}_{\mathbf{q}}$  can be obtained numerically. The dispersion curves for  $D = 0.2$  and  $D = 1.0$  along  $[1\ 0]$  direction has been shown in

Figs.(2) and (3), respectively. As can be seen from these graphs, all the degeneracies have been removed, so we were left with 6 distinct modes, where the highest mode has a maximum at  $q = 0$  with the value  $\lambda_0^1 = -2J + 2D$ . It can be easily shown, by deriving the eigenvector of this mode, that this mode corresponds to all-in all-out spin configuration represented in Fig.(4). As a result, the mean-field theory predicts a continuous phase transition from disordered to a long-range ordered all-in all-out state at the critical temperature  $T_c = -J + D$ . Another interesting point is that the branch  $\lambda_{\mathbf{q}}^4$  is independent of magnitude of anisotropy ( $D$ ), which means that the modes describing by it, are corresponding to spin fluctuations perpendicular to easy-axes directions ( $\hat{z}^a, a = 1, 2, 3$ ) in Hamiltonian, given by Eq.(2).

### III. MONTE CARLO SIMULATION

For large values of  $D$ , spins tend to remain mainly along easy-axes directions such that the effective degrees of freedom flip along these axes. Therefore, one expects that the transition to all-in all-out state to be in 2D Ising universality class. However, when  $D$  is small, the transverse fluctuations normal to local easy-axes directions become larger and so this leads to lowering of the transition temperature as well as deviation from Ising behaviour. In this section we use Monte Carlo simulation, to study the phase transition of the model described in previous section and find the order of transitions for different values of anisotropic term  $D$ .

To obtain a qualitative picture of the transitions and also the approximate location of the critical points, we first set some low resolution simulations. The simulations were carried out using standard Metropolis single spin-rotating algorithm with lattice size  $N = 3 \times 20 \times 20$ . During each simulation step, the angles of planar spins with the horizontal axes were treated as unconstrained, continuous variables. The random-angles rotations were adjusted in such a way that roughly 50% of the attempted angle rotations were accepted. To ensure thermal equilibrium, 100 000 Monte Carlo steps (MCSs) per spin were used for each temperature

and 200 000 MCS were used for data collection. The basic thermodynamic quantities of interest are the specific heat  $c = (\langle E^2 \rangle - \langle E \rangle^2)/(NT^2)$ , the order parameter defined as  $M = |\sum_{i,a} \mathbf{S}_i^a \cdot \hat{z}^a|/N$  and the susceptibility  $\chi = (\langle M^2 \rangle - \langle M \rangle^2)/(NT)$ .

In Figs. (5-8), temperature dependence of the energy per spin, the order parameter, specific-heat and susceptibility have respectively been represented for  $J = -1.0$ ,  $D = 0.2, 0.1$ . As can be observed from Figures.(7) and (8), the transition for  $D = 0.2$  seems to be continuous, while for  $D = 0.1$ , because of sudden peaks in specific heat and susceptibility, it seems to be first order. However, The determination of the order of transition requires more accurate methods, for which we will use Binder's fourth energy cumulant method. Once the probability density of energy ( $P(E, T)$ ) is obtained, for measuring the thermodynamic quantities other than the energy, one can choose to work with this energy probability distribution and microcanonical averages of the quantities of interest. This leads to optimized use of computer memory. The microcanonical average of a given quantity  $A$ , which is a function of energy, can be calculated directly as:

$$A(E) = \frac{\sum_t A_t \delta_{E_t, E}}{\sum_t \delta_{E_t, E}}, \quad (32)$$

from which, the canonical average of  $A$  can be obtained as a function of  $T$ :

$$\langle A \rangle = \frac{\sum_E A(E) P(E, T)}{\sum_E P(E, T)}. \quad (33)$$

In our simulation, we use Kagomé lattices with linear sizes  $L = 20, 24, 28, 32, 36, 40$  (the number of sites is given by  $N = 3 \times L \times L$ ), such that the maximum number of spins is 4800, large enough for reducing the finite size effects. For each system size, at least five overlapping energy histograms are obtained near the transition point so that the statistical uncertainty in the wing of the histograms, may be suppressed by using the optimized multiple-histogram method [28]. This enables us to measure the location and magnitude of the extrema of the thermodynamic quantities with high accuracy. For each histogram we performed  $5 \times 10^5$  Monte Carlo steps per spin for equilibration and also  $5 \times 10^5$  MCSs for gathering data. To reduce the correlation, 10 to 20 Monte Carlo sweeps were discarded between successive

measurements. In all simulation we fix  $J = -1$  and vary the value of  $D$  from 0.1 to 1.0. First of all, we deal with the order of transitions.

### A. Order of the transition

To determine the order of transitions, we used Binder's fourth energy cumulant defined as:

$$U_L = 1 - \frac{\langle E^4 \rangle}{3 \langle E^2 \rangle^2}. \quad (34)$$

It has been shown that this quantity reaches a minimum at the effective transition temperature  $T_c(L)$  whose size dependence is given by [29–31]:

$$U_{min}(L) = U^* + BL^{-d} + O(L^{-2d}), \quad (35)$$

where

$$U^* = \frac{2}{3} - (e_1/e_2 - e_2/e_1)^2 / 12. \quad (36)$$

The quantities  $e_1$  and  $e_2$  are the values of energy per site at the transition point of a first order phase transition and  $d$  is the spatial dimension of the system ( $d = 2$  in our simulation). Hence, for the continuous transitions for which there is no latent heat ( $e_1 = e_2$ ), in the limit of infinite system sizes,  $U_{min}(L)$  tends to the value  $U^*$  equal to  $2/3$ . For the first-order transitions, however  $e_1 \neq e_2$  and then  $U^*$  reaches a value less than  $2/3$  in the the limit  $L \rightarrow \infty$ .

The size dependences of  $U(L)$  for  $D = 1.0, 0.18, 0.15, 0.13, 0.1$  have been exhibited in Fig.(9). The straight lines fitted to the data have been obtained from Eq.(35). The values of  $U^*$  and latent heat per spin are also listed in Table.(I), from which one can see that, within the errors of simulation, transitions are second order for  $D > 0.17$  and clearly first order for  $D < 0.15$ . The precise determination of the tricritical point is extremely difficult, however our results suggest the existence of a tricritical point between  $D/|J| = 0.15$  and  $D/|J| = 0.17$ .

In the Figs.(10) and (11) the energy histograms of  $D = 0.2$  and  $D = 0.1$  for the size  $N = 3 \times 40 \times 40$  have been shown, respectively. As can be seen from these figures, the energy histogram for  $D = 0.2$  has one broad peak at the transition, while for  $D = 0.1$ , it has two well separated peaks around the transition temperature. This is in agreement with the results of Binder's method. Note that the small peak at the middle in Fig.(11), is artifact of the finite time of simulation and will vanish at large enough times. The reason is that at a strong first order transition point, free energy possesses two equivalent minima corresponding to two stable coexisting phases. For large system sizes these two minima are separated by a large energy barrier, so the system remains mainly around its minima during the time evolution, caused by thermal fluctuations, in simulation. Therefore, the configurations corresponding to the unstable region at the middle are rare, consequently the relative error for these data is large.

As the next step we proceed to calculate the critical temperatures and critical exponents for continuous phase transitions, using finite-size scaling theory.

## B. Determination of $T_c$ and static critical exponents

According to the finite-size scaling theory [32], the scaling form for various thermodynamic quantities such as magnetization density, susceptibility and specific heat in zero field are given by:

$$m \approx L^{\beta/\nu} \mathcal{M}(tL^{1/\nu}) \quad (37)$$

$$\chi \approx L^{\gamma/\nu} \mathcal{K}(tL^{1/\nu}) \quad (38)$$

$$c \approx c_\infty(t) + L^{\alpha/\nu} \mathcal{C}(tL^{1/\nu}), \quad (39)$$

where  $t = (T - T_c)/T_c$  is the reduced temperature for a sufficiently large system at a temperature  $T$  close enough to the infinite lattice critical point  $T_c$ ,  $L$  is the linear size of the system and  $\alpha, \beta, \gamma, \delta$  are static critical exponents. Equations (37-39) are used to estimate the critical exponents. However, before dealing with the critical exponents we should first

determine the critical temperature accurately.

The logarithmic derivatives of total magnetization ( $mL^d$ ) are important thermodynamic quantities for studying critical phenomena and very useful to high accurate estimation of the critical temperature  $T_c$  and the correlation length critical exponent ( $\nu$ ) [33]. To this, we Define the following quantities:

$$V_1 \equiv 4[M^3] - 3[M^4], \quad (40)$$

$$V_2 \equiv 2[M^2] - [M^4], \quad (41)$$

$$V_3 \equiv 3[M^2] - 2[M^3], \quad (42)$$

$$V_4 \equiv (4[M] - [M^4])/3, \quad (43)$$

$$V_5 \equiv (3[M] - [M^3])/2, \quad (44)$$

$$V_6 \equiv 2[M] - [M^2], \quad (45)$$

where  $M = Nm$  is the total magnetization of the system and

$$[M^n] \equiv \ln \frac{\partial \langle M^n \rangle}{\partial T}. \quad (46)$$

From Eq.(37) it is easy to show that

$$V_j \approx (1/\nu) \ln L + \mathcal{V}_j(tL^{1/\nu}), \quad (47)$$

for  $j = 1, 2, \dots, 6$ . At the critical temperature ( $t = 0$ ),  $\mathcal{V}_j$  should be constants, independent of the system size  $L$ . Using Eq. (47) one can find the slope of quantities  $V_1$  to  $V_6$  (Eq. 40-45) versus  $\ln(L)$  for the region near the critical point. Scanning over the critical region and looking for a quantity-independent slope gives us both the critical temperature  $T_c$  and the correlation length exponent  $\nu$  with high precision. Figures (12) and (13) give the examples of such an effort for the set of the coupling  $D/|J| = 0.2$ . From these figures, we estimate that  $\nu = 0.842(2)$  and  $T_c = 1.198(1)$ . The linear fits to the data in Fig.(12) have been obtained by the linear least squares method.

Once  $\nu$  and  $T_c$  are determined accurately, we can extract other static critical exponents related to the order parameter ( $\beta$ ) and susceptibility ( $\gamma$ ). The ratio  $\beta/\nu$  can be estimated

by using the size dependence of the order parameter at the critical point given by Eq.(37). Fig.(14) shows the log-log plots of the size dependence of the order parameter corresponding to  $D/|J| = 0.5$  and  $D/|J| = 0.2$ . From this figure the ratio  $\beta/\nu$  can be estimated as the slope of the straight lines fitted to the data according to Eq.(37). We then have  $\beta/\nu = 0.198(8)$  for  $D/|J| = 0.5$  and  $\beta/\nu = 0.285(8)$  for  $D/|J| = 0.2$ .

Accordingly, from Eq.(38) it is clear that the peak values of the finite-lattice susceptibility ( $\chi = (\langle M^2 \rangle - \langle M \rangle^2)/(NT)$ ) and the magnitude of the true susceptibility at  $T_c$  (the same as  $\chi$  with  $\langle m \rangle = 0$ ) are asymptotically proportional to  $L^{\gamma/\nu}$ . Then the slope of straight line fitted linearly to the log-log plot of these two quantities versus linear size of the lattices, can be calculated to estimate the ratio  $\gamma/\nu$ . In Fig.(15) the finite lattice susceptibility have been depicted for  $D/|J| = 0.2, 0.5$ , respectively. The slopes of linear lines fitted to these data give  $\gamma/\nu = 1.39(2)$  for  $D/|J| = 0.5$  and  $\gamma/\nu = 1.42(2)$  for  $D/|J| = 0.2$ , where the error includes the uncertainty in the slope resulting from uncertainty in our estimate for  $T_c$ .

The above procedure has been applied for other values of  $D/|J| = 1.0, 0.5, 0.2$  and the obtained critical exponents are listed in Table.(II). In this table, the critical exponent  $\alpha$ , has been calculated using the hyper-scaling relation:

$$\alpha = 2 - d\nu, \quad (48)$$

in which  $d = 2$ . On the other hand the Rushbrook scaling law ( $\alpha + 2\beta + \gamma = 2$ ) is satisfied for all set of exponents within the computational errors. For comparison, we have listed the corresponding critical exponents of Onsager's solution for 2D-Ising, and also Zamolodchikov's conjecture for the Ising-tricritical point in two-dimensions, which corresponds to a 2D- $\phi^6$  field theory [34]. Zamolodchikov's conjecture is based on conformal field theory and has been verified by Monte Carlo simulation [35].

One can see from Table.(II) that the critical exponents for  $D/|J| = 1.0$  are pretty close to the 2D-Ising values, then anisotropy magnitude of  $D/|J| = 1.0$  is large enough to suppress the transverse fluctuations normal to easy-axes directions. Upon decreasing the anisotropy, the transverse fluctuations become important and the exponents deviate from Ising values.

However, although the exponents  $\nu$ ,  $\gamma$  and  $\alpha$  monotonously tend to the 2D-tricritical values, but the exponent  $\beta$  gets farther from it. This discrepancy, might the sign of a new universality class, other than 2D- $\phi^6$  model.

At the end, we deal with the dependence of the transition temperature to the anisotropy intensity. We have already mentioned the method of obtaining the critical temperature for the continuous transitions ( $D > 0.17$ ). For strongly enough first order transitions whose energy histograms are double peaked ( $D < 0.15$ ), the finite size transition temperatures ( $T_c(L)$ ), are determined as the temperature at which the two peaks have equal heights. Once  $T_c(L)$  for all lattice sizes is obtained, the transition temperature in thermodynamic limit can be extrapolated by the following scaling relation:

$$T_c(L) = T_c(\infty) + BL^{-d}, \quad (49)$$

where  $B$  is a constant and  $d = 2$ . The resulting transition temperatures are listed in Table.(I). In Fig.(16), we have plotted the transition temperature versus  $D$  in logarithmic scale. This linear log-log plot shows a power law relation between these two quantities as:

$$T_c \propto D^{0.501(2)}. \quad (50)$$

This result is in clear contrast with mean-field prediction of a linear dependence of transition temperature on the anisotropy intensity  $D$ . This scaling behaviour can be explained by a simple dimensional analysis. Assuming that both exchange interaction,  $J$ , and anisotropy,  $D$ , are equally important in occurrence phase transition in  $XY$  Kagomé antiferromagnet. So the thermal energy which balances the entropy and internal energy at the transition point, must be proportional to a combination of  $J$  and  $D$ . Accordingly, dimensional analysis requires  $K_B T_c \sim (|J|D)^{\frac{1}{2}}$ , which leads us to  $T_c/|J| \sim (D/|J|)^{\frac{1}{2}}$ .

#### IV. CONCLUSION

In summary, using mean-field theory and the optimized Monte Carlo simulation based on multi-histogram, we investigated the phase transitions of the antiferromagnetic classical  $XY$



model on a two dimensional Kagomé lattice with the easy-axes single ion anisotropy. In the absence of anisotropy, this system is highly frustrated and no phase transition is expected to occur at finite temperatures, except the Kosterlitz-Thouless transition mentioned in Ref. [24]. Turning on the anisotropy, removes the degeneracies of the ground state and so establishes a long range order with all-in all-out spin configuration at low temperatures. By increasing the temperature, the system exhibits a phase transition from all-in all-out ordered state to disordered (paramagnetic) state. According to Monte Carlo results this transition is first order for small values of anisotropy, while turns to second order at a tricritical point, corresponding to an anisotropy strength in the interval  $0.15 < \frac{D}{|J|} < 0.17$ .

Employing finite size scaling theory, we derived the critical exponents for continuous transitions and found that the transition is in Ising universality for large values of anisotropy. This is because in large  $D/|J|$  limit, the fluctuations perpendicular to easy-axes directions are frozen, and so the effective degrees of freedom are spin flips along easy-axes directions, such that the order parameter possess the discrete  $Z_2$  symmetry. Decreasing the anisotropy magnitude, activates the spin fluctuations perpendicular to the easy-axes directions. In principle, the coupling of transverse modes (independent of anisotropy) and also of other underlying modes, shown in Fig.(2) and (3), with the all-in all-out state at  $q = 0$ , is the reason for the deviation of the universality class of transitions from Ising, and is also responsible for changing the type of transition to dis-continuous for small values of anisotropy. However, obtained critical exponents near the tricritical point, do not coincide with those of two-dimensional Ising-tricritical point derived from 2D- $\phi^6$  field theory. This suggests the possibility of the existence of a new tricritical universality class in two-dimensions. It is not surprising, because the critical behaviours in frustrated systems are usually different from standard universality classes [36]. In this case, finding such a universality class requires more theoretical and numerical investigations.

We hope that this work will motivate further experimental, computational and analytical efforts for deeper understanding of the nature of transitions in geometrically frustrated

systems.

### **Acknowledgment**

We would like to thank M. J. P. Gingras, H. Kawamura, and P. Holdsworth for enthusiastic discussions and useful comments.

# TABLES

$D/J$	$T_c$	$U^*$
1.0	0.449(1)	0.66662(7)
0.5	0.316(1)	0.66660(9)
0.2	0.199(1)	0.66659(8)
0.18	0.189(5)	0.66653(9)
0.17	0.184(6)	0.66649(9)
0.15	0.174(8)	0.6664(1)
0.14	0.167(7)	0.6662(1)
0.13	0.162(7)	0.6661(1)
0.12	0.156(8)	0.6659(1)
0.1	0.142(8)	0.6658(1)

TABLE I. The critical temperatures and value of  $U^*$  for  $\frac{D}{J} = 1.0, 0.5, 0.2, 0.18, 0.17, 0.15, 0.14, 0.13, 0.12, 0.1$ . (see the text)

$D/ J $	$\nu$	$\beta$	$\gamma$	$\alpha$	$\alpha + 2\beta + \gamma$
1	1.019(2)	0.15(1)	1.64(8)	-0.038(4)	1.9(1)
0.5	0.959(2)	0.19(1)	1.52(6)	0.082(4)	2.0(1)
0.2	0.842(2)	0.24(2)	1.18(6)	0.316(4)	2.0(1)
2D-Ising	1	1/8	7/4	0(log)	2
2D- $\phi^6$	5/9	1/24	37/36	8/9	2

TABLE II. The static critical exponents  $\nu, \beta, \gamma$  and  $\alpha$  for  $\frac{D}{J} = 1.0, 0.5, 0.2$ , derived from finite-size scaling. In the last column the Rushbrook's scaling law is computed. The last two rows are listed the corresponding exact critical exponent of 2D-Ising model and two-dimensional Ising-tricritical point, respectively.

## REFERENCES

- [1] J. E. Greedan, Chem. Mater. **11**, 37 (2001).
- [2] A. P. Ramirez, Annu. Rev. Mater. Sci. **24**, 453 (1994).
- [3] P. Schiffer, and A. P. Ramirez, Comments Cond. Matter Phys. **18**, 21 (1996).
- [4] R. Moessner, Can. J. Phys. **79**, 1283 (2001).
- [5] S. Kondo *et al*, Phys. Rev. Lett. **78**, 3729 (1997).
- [6] A. Ramirez, A. Hayashi, R. J. Cava, R. Siddharthan, B. S. Shastry, Nature **399**, 333 (1999).
- [7] J. Snyder, J. S. Slusky, R. J. Cava, and P. Schiffer, Nature **413**, 48 (2001).
- [8] S. T. Bramwell, and M. J. P. Gingras, Science **294**, 1495 (2001).
- [9] J. T. Chalker, P. C. W. Holdsworth, and E. F. Shender, Phys. Rev. Lett. **68**, 855 (1992).
- [10] C. Waldtmann, H.-U. Everts, B. Bernu, C. Lhuillier, P. Sindzingre, P. Lecheminant, and L. Pierre, Eur. Phys. J. B **2**, 501 (1998).
- [11] S. Sachdev, Phys. Rev. B **45**, 12377 (1992).
- [12] C. Zeng, and V. Elser, Phys. Rev. B **51**, 8318 (1995).
- [13] M. Hanawa, Y. Muraoka, T. Tayama, T. Sakakibara, J. Yamaura, and Z. Hiroi, Phys. Rev. Lett. **87**, 187001 (2001).
- [14] J. Villain, Z. Phys. B **33**, 31 (1978).
- [15] R. Moessner, and J.T. Chalker, Phys. Rev. Lett. **80**, 2929 (1998); R. Moessner, and J.T. Chalker. Phys. Rev. B **58**, 12049 (1998); R. Moessner, D.Phil. thesis, Oxford University. 1996.
- [16] J.N. Reimers, Phys. Rev. B **45**, 7287 (1992); M.P. Zinkin, M.J. Harris, and T. Zeiske,

- Phys. Rev. B **56**, 11786 (1997).
- [17] G. Ferey, R. De Pape, M. Leblanc, and J. Pannetier, Rev. Chem. Min. **23**, 474 (1986).
  - [18] J. N. Reimers, J. E. Greedan, C. V. Stager, M. Björgvinnsen, and M. A. Subramanian, Phys. Rev. B **43**, 5692 (1991).
  - [19] J. N. Reimers, A. J. Berlinsky and A. C. Shi, Phys. Rev. B **43**, 865 (1991)
  - [20] J. N. Reimers, J. E. Greedan, and M. Björgvinsson, Phys. Rev. B **45**, 7295 (1992).
  - [21] P. Holdsworth, and E. Loyer, private communications.
  - [22] H. Kawamura, private communications.
  - [23] D. A. Huse, and A. D. Rutenberg, Phys. Rev. B **45**, 7536 (1992).
  - [24] I. Ritchey, P. Chandra, and P. Coleman, Phys. Rev. B **47**, 15342 (1993).
  - [25] J. N. Reimers, and A. J. Berlinsky, Phys. Rev. B **48**, 9539 (1993).
  - [26] S. T. Bramwell, M. J. P. Gingras, and J. N. Reimers, J. Appl. Phys, **75**, 5523 (1994).
  - [27] A. B. Harris, O. G. Mouritson, and A. J. Berlinsky, Can. J. Phys **62**, 915 (1984).
  - [28] A. M. Ferrenberg, and R. H. Swendsen, Phys. Rev. Lett, **63**, 1195 (1989).
  - [29] M. S. S. Challa, D. P. Landau, and K. Binder, Phys. Rev. B, **34**, 1841 (1986).
  - [30] J. Lee, and J. M. Kosterlitz, Phys. Rev. B, **43**, 3265 (1991).
  - [31] D. P. Landau, and K. Binder, *A guide to Monte Carlo simulations in statistical physics*, (Cambridge university press, 2000)
  - [32] M. N. Barber, *Phase transitions and critical phenomena*, edited by C. Domb and J. L. Lebowitz (Academic, New York, 1983), Vol. 8, p. 145.
  - [33] K. Chen, A.M. Ferrenberg, and D. P. Landau, Phys. Rev. B, **48**, 3249 (1993).

- [34] A. B. Zamolodchikov, Sov. J. Nucl. Phys. 44, 529 (1986).
- [35] M. Asorey, J. G. Esteve, F. Falceto, and J. Salas, Phys. Rev. B, **52**, 9151 (1995).
- [36] H. Kawamura, J. Phys: Condens. Matter, **10**, 4707 (1998).

# FIGURES

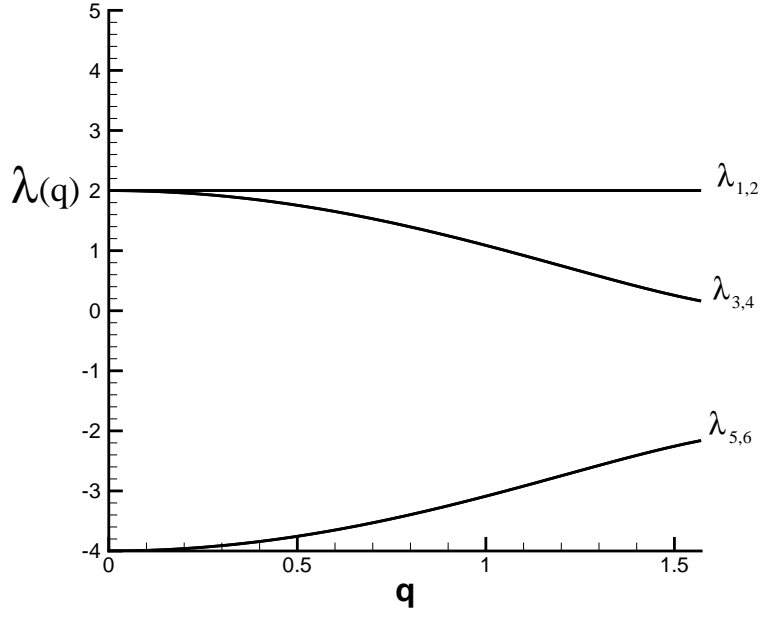


FIG. 1. spectrum of coupling matrix  $\tilde{J}$  for  $D = 0$  along  $[10]$  direction. Each branch has two fold degeneracy.

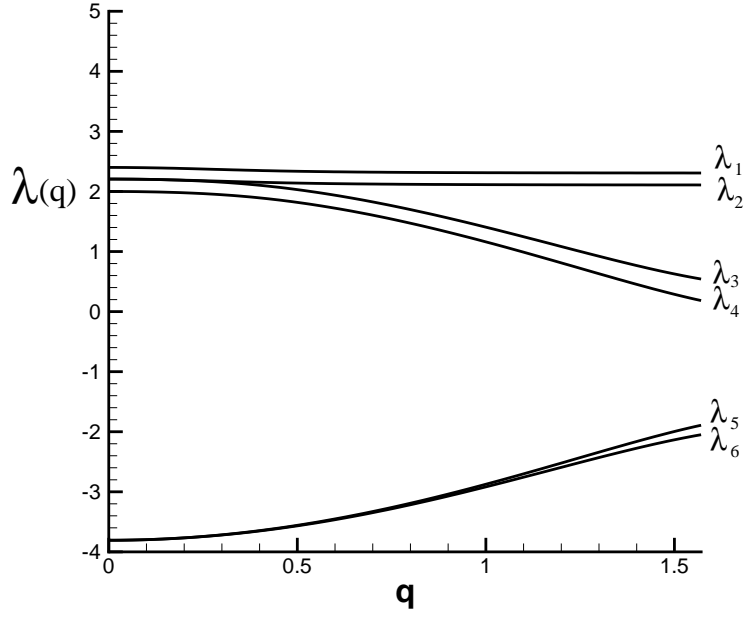


FIG. 2. spectrum of coupling matrix  $\tilde{J}$  for  $D = 0.2$  along  $[10]$  direction. degeneracies have been removed by addition anisotropic term.



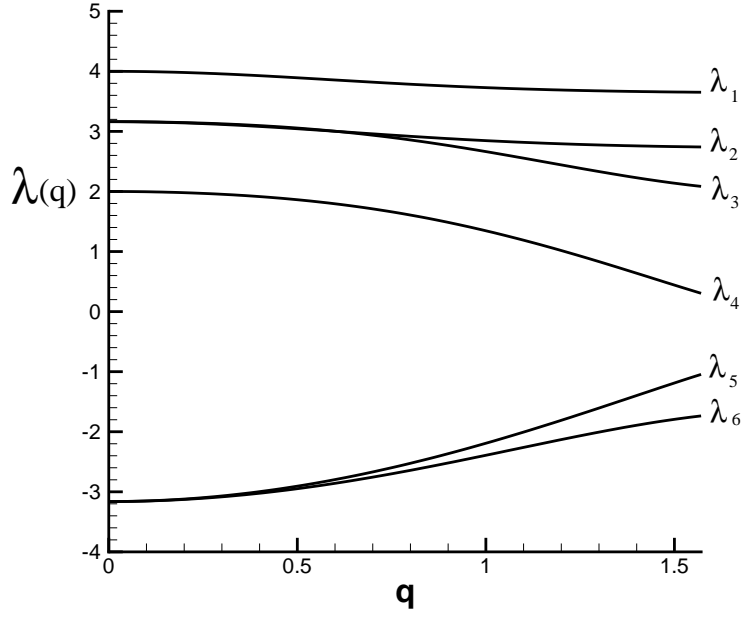


FIG. 3. spectrum of coupling matrix  $\tilde{J}$  for  $D = 1.0$  along  $[10]$  direction. degeneracies have been removed by addition anisotropic term.

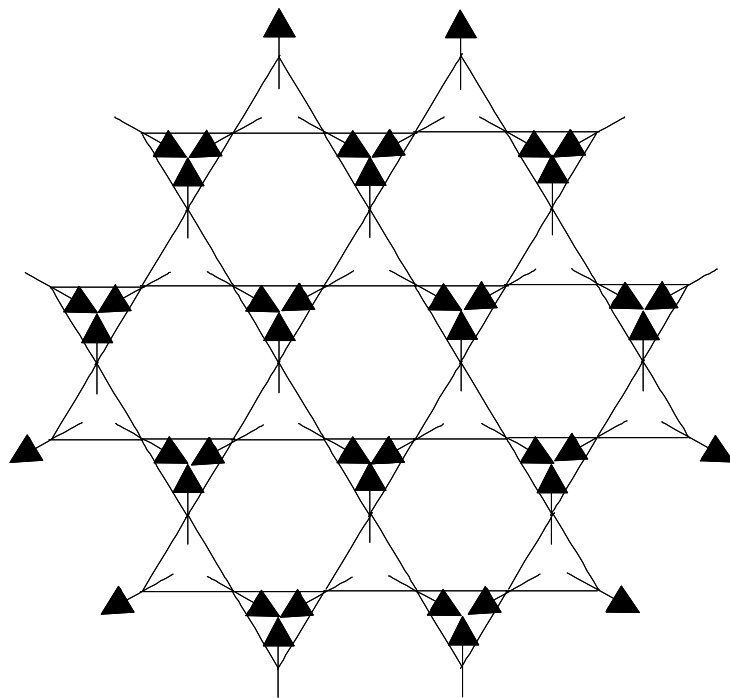


FIG. 4. All in-all out configuration in kagome' lattice.

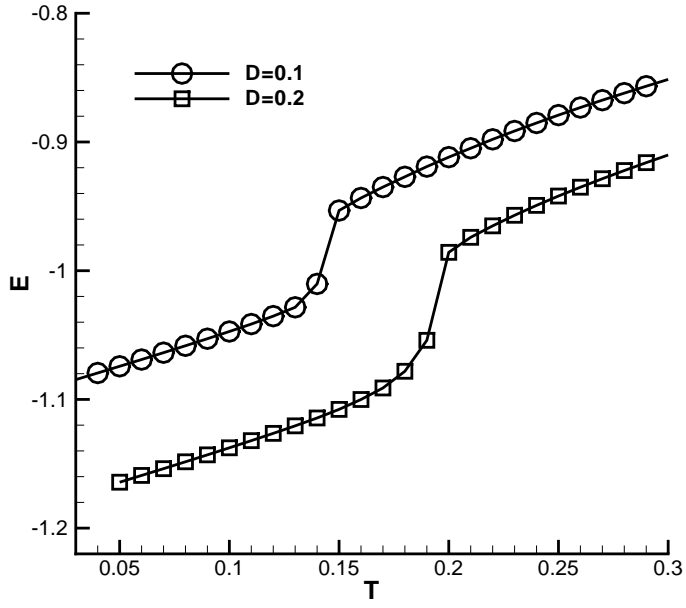


FIG. 5. Temperature dependence of Energy per spin for  $D = 0.2, 0.1$ .

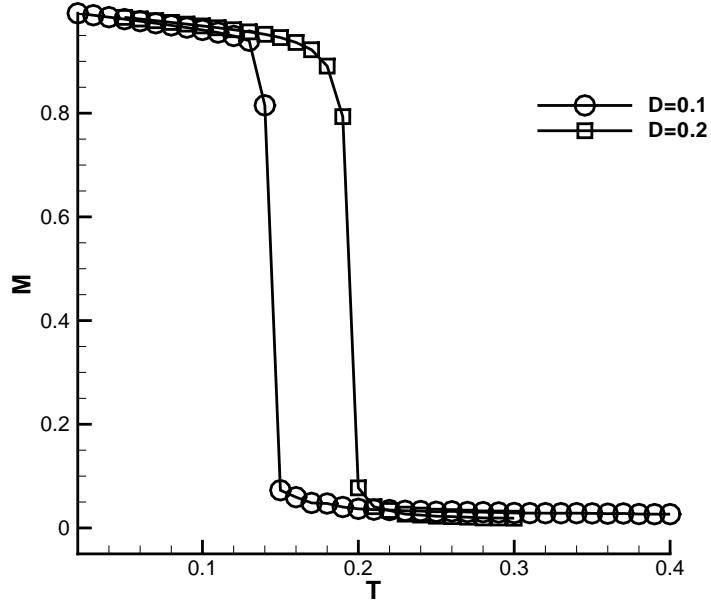


FIG. 6. Temperature dependence of order parameter(magnetization) for  $D = 0.2, 0.1$ .

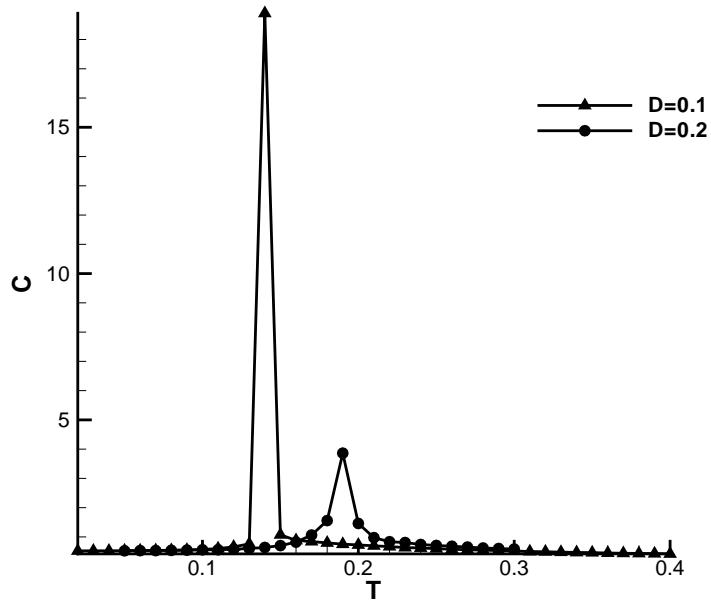


FIG. 7. Temperature dependence of specific heat for  $D = 0.2, 0.1$ .

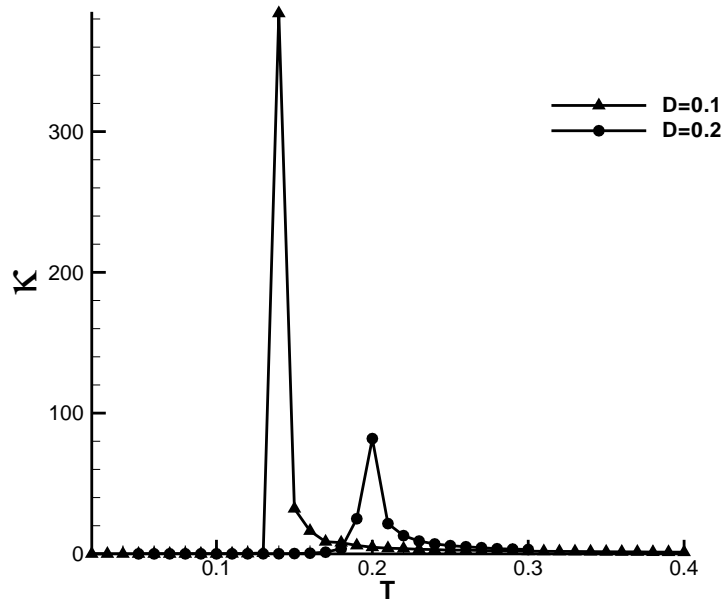


FIG. 8. Temperature dependence of susceptibility for  $D = 0.1, 0.2$ .

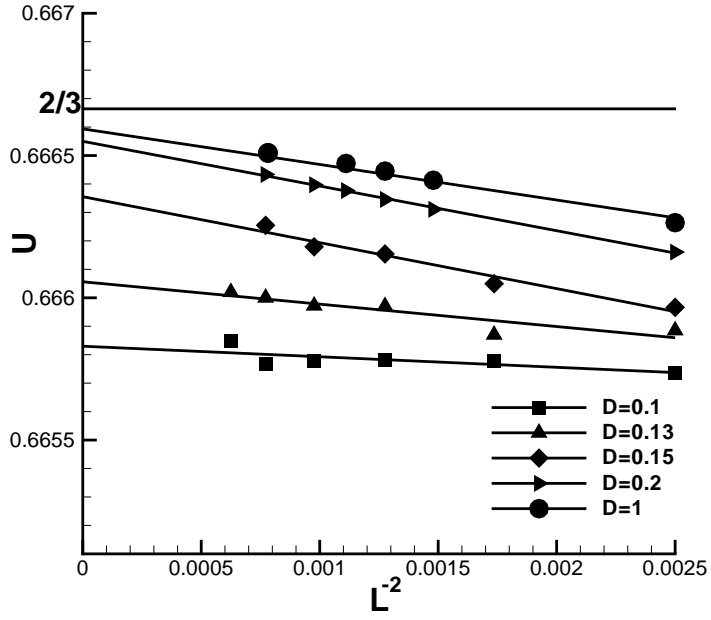


FIG. 9. Size dependences of binder's fourth energy cumulant for  $D = 1.0, 0.2, 0.15, 0.13, 0.1$ .

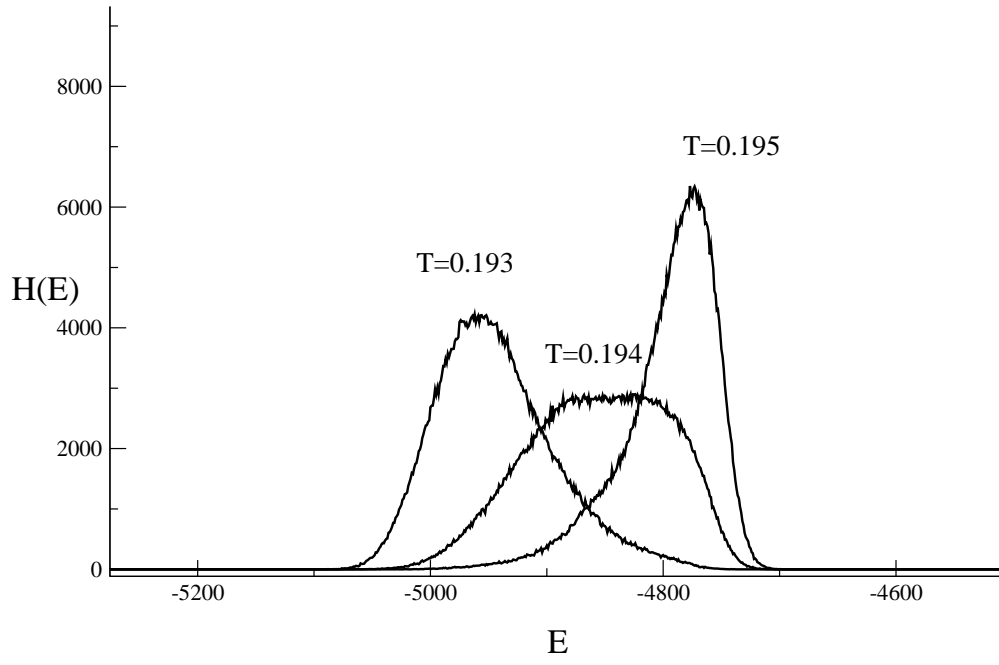


FIG. 10. Three energy histograms for  $D = 0.2$  and size  $N = 3 \times 40 \times 40$  near the transition temperature.



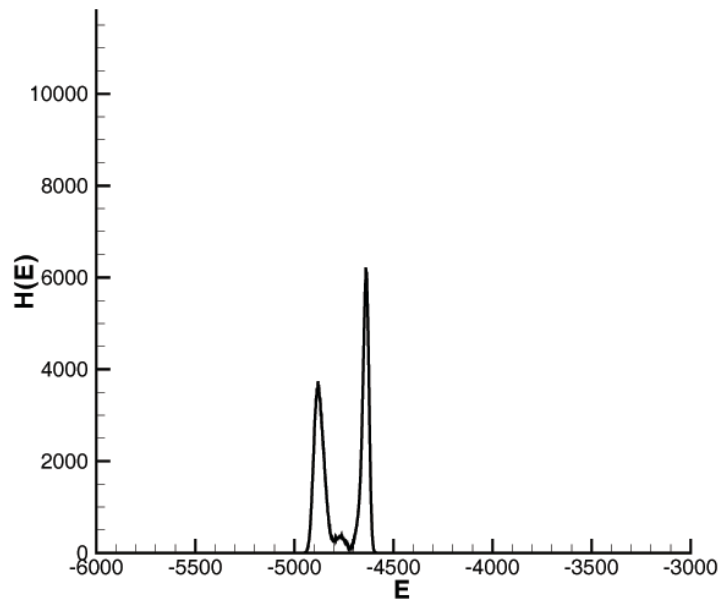


FIG. 11. Energy histogram for  $D = 0.1$  and size  $N = 3 \times 40 \times 40$  near the transition temperature.

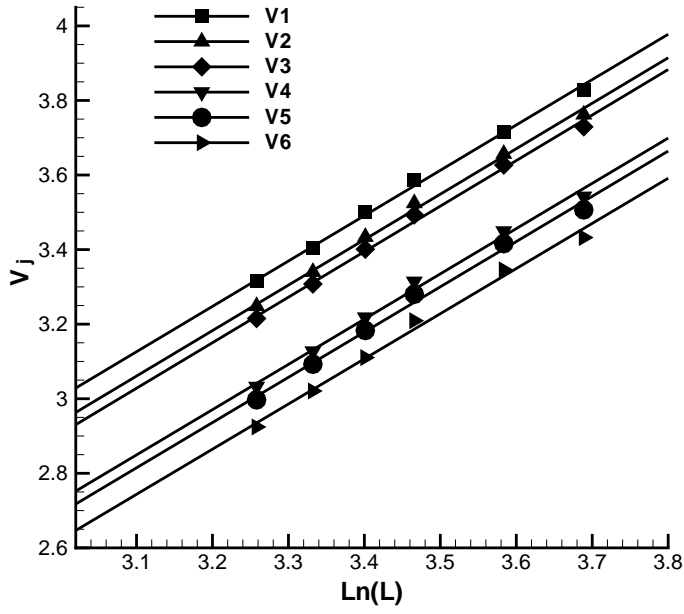


FIG. 12. Dependence of quantity  $V_j$  (see the text) versus logarithm of  $L$  for  $D = 0.2$  at  $T = 0.1989(5)$ . The solid lines represent linear fits to Eq.(47). All straight lines have the same slope  $\nu = 0.842(2)$ .

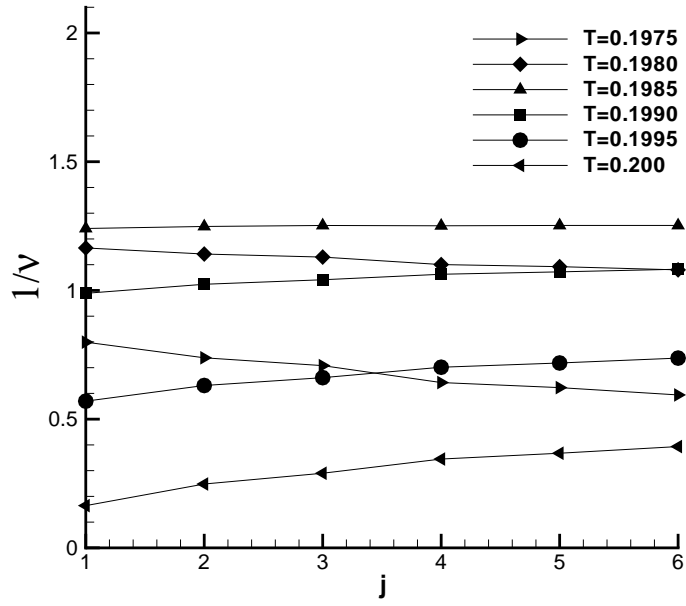


FIG. 13. Scanning results for the dependence of quantity  $V_j$  versus  $j$  for  $D = 0.2$ . The horizontal line is drawn at  $1/\nu = 1.187$ .

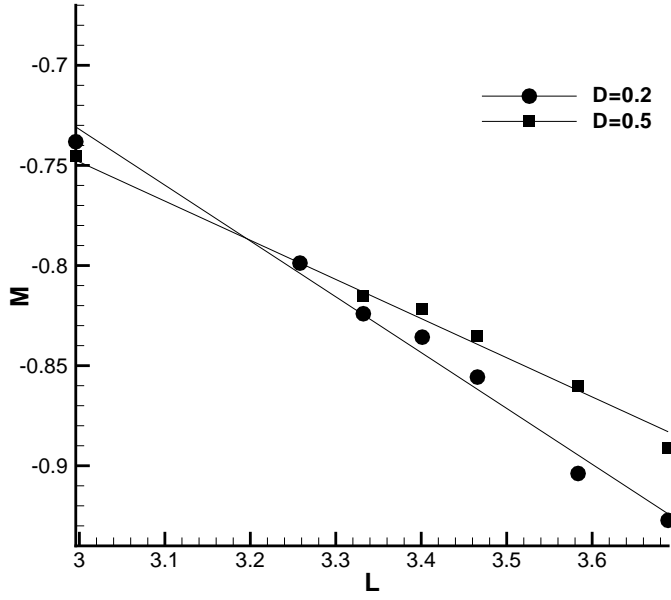


FIG. 14. Log-Log plot of order parameter for  $D = 0.5, 0.2$ . The slopes of fitted line gives  $\frac{\beta}{\nu} = 0.285(7)$  for  $D = 0.2$  and  $\frac{\beta}{\nu} = 0.198(8)$  and for  $D = 0.5$ .

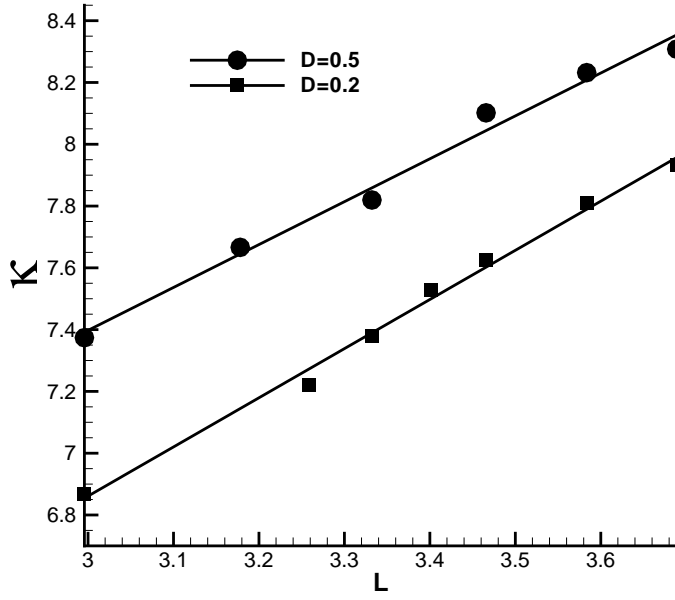


FIG. 15. Log-Log plot of finite lattice susceptibility for  $D = 0.2, 0.5$ . The slopes of fitted lines give  $\frac{\gamma}{\nu} = 1.58(5)$  for  $D = 0.2$  and  $\frac{\gamma}{\nu} = 1.40(5)$  for one  $D = 0.5$ .

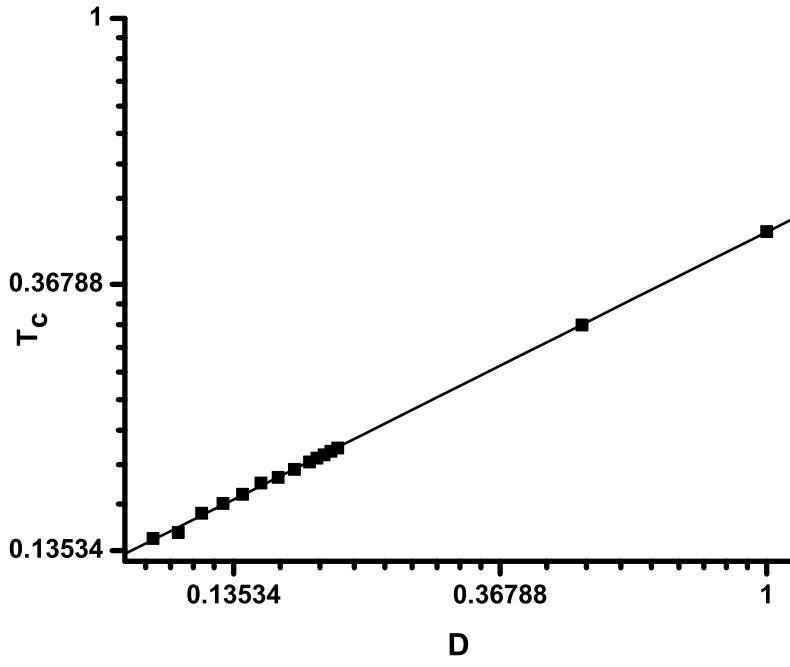


FIG. 16. Log-Log plot of transition temperature versus anisotropy magnitude  $D$ . The slope of fitted line is  $0.501(2)$ .